Plasmonics (2009) 4:209–216
DOI 10.1007/s11468-009-9094-2

Optical Biochip with Multichannels for Detecting Biotin–Streptavidin Based on Localized Surface Plasmon Resonance

Shaoli Zhu · Yongqi Fu

Received: 17 March 2009 / Accepted: 11 May 2009 / Published online: 27 May 2009

Abstract A rapid and accurate detection of molecular binding of antigen-antibody signaling in high throughput is of great importance for biosensing technology. We proposed a novel optical biochip with multichannels for the purpose of detection of biotin–streptavidin on the basis of localized surface plasmon resonance. The optical biochip was fabricated using photolithography to form the microarrays functioning with multichannels on glass substrate. There are different nanostructures in each microarray. Dry etching and nanosphere lithography techniques were applied to fabricate Ag nanostructures such as hemispheres, nanocylindricals, triangular, and rhombic nanostructures. We demonstrated that 100-nM target molecule (streptavidin) on these optical biochips can be easily detected by a UV-visible spectrometer. It indicated that period and shape of the nanostructures significantly affect the optical performance of the nanostructures with different shapes and geometrical parameters. Our experimental results demonstrated that the optical biochips with the multichannels can detect the target molecule using the microarrays structured with different shapes and periods simultaneously. Batch processing of immunoassay for different biomolecular through the different channels embedded on the same chip can be realized accordingly.

S. Zhu (✉)
School of Electronic and Electrical Engineering,
Nanyang Technological University,
Singapore, Singapore
e-mail: slzhu@ntu.edu.sg

Y. Fu
School of Physical Electronics,
University of Electronic Science and Technology of China,
Chengdu 610054, Sichuan Province, People's Republic of China

Keywords Localized surface plasmon resonance · Multichannel nanosensing · Spectroscopy · Biochip

Introduction

Recently, biochemical nanosensor is an active research topic in both life sciences and engineering [1]. It involves the interdisciplinary areas of life sciences and information sciences such as bioinformatics, biochemistry chip, biocybernetics, bionics, and biocomputer. Their common characteristics are exploring and opening out the basic rules of the production, storage, transmission, process, transition, and control of information in the biological systems, as well as discussing the basic methods which are employed for the human economy activity. The biosensor-related research focuses on combination of the sensors and the diversified biologically active materials as well as their relevant applications.

Localized surface plasmon resonance (LSPR)-based nanosensors become hot research spot because many researchers have begun development situation and important position in the life sciences research [2–8]. The LSPR nanosensors can be implemented using extremely simple, small, light, robust, and low-cost equipments. It has many advantages such as convenience, high sensitivity, wide application, and real-time detection. Thus, it is deemed to be a type of high potential biosensor. Optical properties of the metal nanoparticles strongly depend on their size, shape, metal composition, and refractive index of the surrounding mediums. Previous research has shown that the LSPR-based nanosensor is a refractive index variation-based sensing device which strongly relies on the extraordinary optical properties of noble (e.g., Ag, Au, and Cu)

metal nanoparticles [9–12]. The Ag nanoparticles have endowed the device with excellent optical properties. Especially, the peak wavelength of the transmittance spectrum λ_{max} is unexpectedly sensitive to the nanoparticles' size, shape, and local external dielectric environment. Its sensitivity to the nanoenvironment has given us the foundation to develop a new serial of affinity biochemosensors in nanoscale.

Miura et al. reported a compact surface plasmon resonance immunosensor using multichannels for detection of small-molecule compounds [13, 14]. Their multichannels are composed of one reference channel and three sensing channels with additional layers with different thickness, on which each ligand is patterned. The sensing is designed on the basis of SPR instead of LSPR, and thus a prism is employed in the system. This causes a complicated system with three limited channels only for the sensing.

In this paper, we presented a multichannel-based optical biochip with different shapes and periods of Ag nanostructure arrays functioning as the biosensors to measure the transmission and extinction spectra originating from these nanoscale Ag particle arrays, as shown in Fig. 1. Signals from the multichannel are generated from the Ag nanoparticle arrays with tunable shapes (e.g., hemisphere, cylindrical, triangular, rhombic, etc.) and periods. It was demonstrated from the experimental results that the nanoparticle array-based LSPR immunosensor with different shapes and periods is capable to be used as an immunosensor. The LSPR-based biochip with the multichannels can realize two specific functions: (1) detecting various biosamples simultaneously in the multichannels and (2) for the same biosample attached on the chip, the effective-refractive-index-matched maximum spectrum corresponding to a certain shape or period particle array can be derived. Moreover, the multichannel-based optical biochip can realize detecting the various targeted molecular using the nanoparticle arrays with different shapes and periods simultaneously. Because a planar biochip was employed to replace the reported prism-based multichannels, our immunosensors have the advantages of simplicity, more detection targets, high throughput,

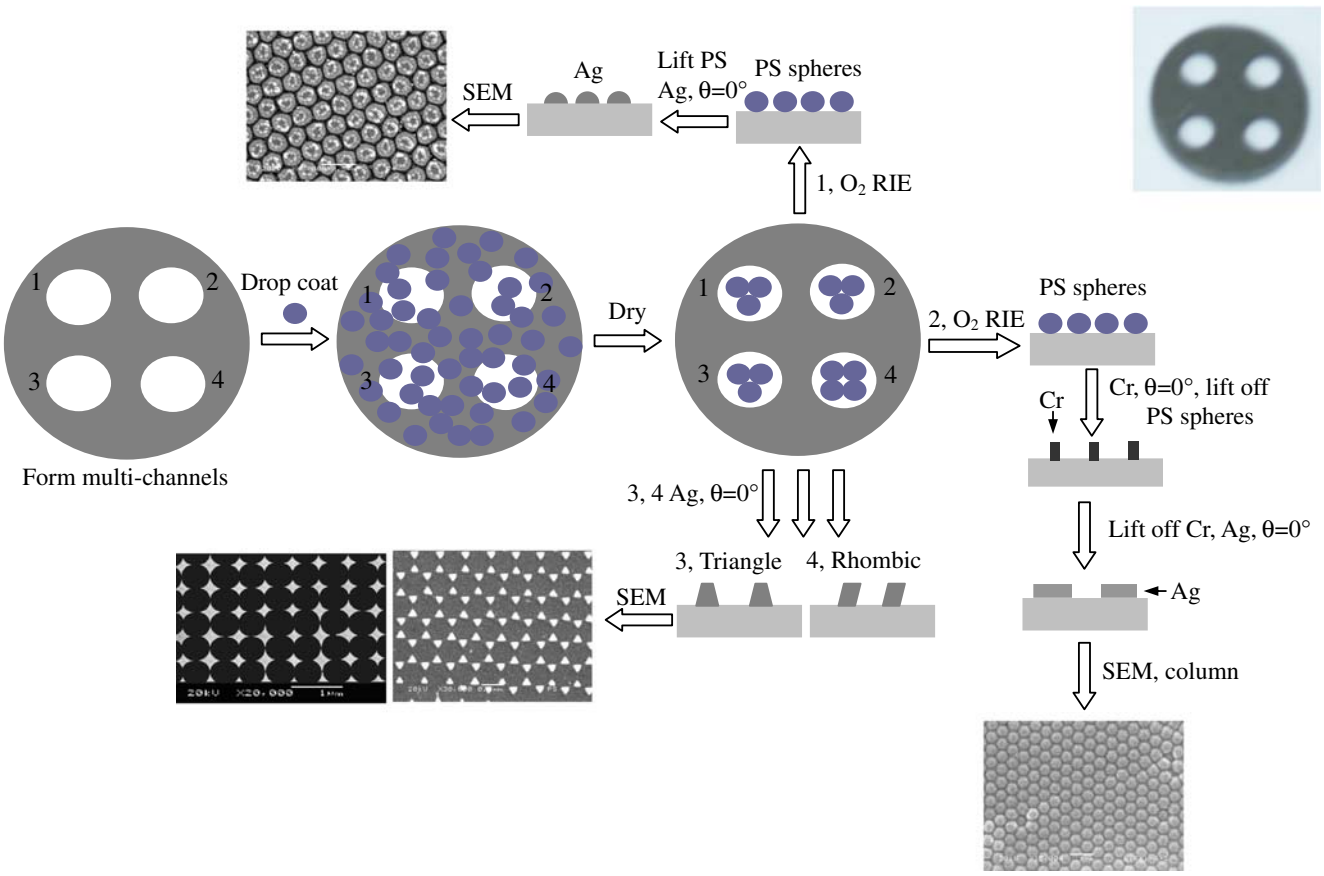

Fig. 1 Flow chart of the nanoparticle preparation. (1) Glass substrates cleaning; (2) monodisperse polystyrene nanospheres are spin-coated and dried; (3) RIE dry etching; (4) Ag metallization by e-beam evaporation; (5) lift off the polystyrene nanospheres; and (6) representative scanning electron microscope image of the chip, *inset* is the picture of the multichannels substrate

etc. in comparison to that of the reported SPR multichannel sensors.

Experiments

Fabrication

Nanosphere lithography (NSL) [12, 15] and reactive ion etching (RIE) techniques were used to create surface-confined different Ag nanoparticle array supported on a glass substrate, as shown in schematic diagram of Fig. 1; inset is the schematic diagram of the multichannel substrate. Firstly, the glass substrate is cleaned using both acid, alkaline, and deionized water. Next, the self-assembly of size monodisperse polystyrene nanospheres forms a deposition mask. Then, the RIE dry etching technique was employed to create the patterns with different shapes. After that, a metal film is deposited through the nanosphere masks using thermal or electron beam evaporation. After removal of the polystyrene nanospheres, well-ordered two-dimensional (2D) nanoparticle arrays remained on the substrate. By changing the diameter of the nanosphere and thickness of the deposited metal film, nanoparticles with different in-plane width, out-of-plane height, and interparticle spacing can be produced. Figure 1 shows the fabrication process of the nanoparticles. In addition, focused ion beam direct milling technique is another option for fabrication of the metallic nanoparticle arrays with different shapes and periods on one chip surface [16, 17].

We measured the surface modality of the samples using JSM-5900LV Scanning Electron Microscope (SEM). In the channels numbered 1, shape of the Ag nanoparticle array is hemisphere. Diameter of the nanohemisphere, out-of-plane heights, and period of array is 440, 30, and 440 nm, respectively. Channel 2 is Ag nanocylindrical array, diameter of the nanocylindrical, out-of-plane heights, and period of array is 450, 40, and 500 nm, respectively. Channel 3 is Ag triangular array, and the out-of-plane heights and period of array is 40 and 440 nm, respectively. Channel 4 is Ag rhombic array, and out-of-plane heights and period of array is 40 and 440 nm, respectively. The external tensility is not symmetrical while carrying out the evaporation process because of the limitation of the self-assembled monolayer (SAM) method. Thus, the size of the Ag nanorhombus is irregular.

Nanoparticle functionalization

To prepare the LSPR nanosensor for the biosensing events, the Ag nanoparticle arrays are firstly functionalized with an SAM composed of 3:1 1-octanethiol (1-OT, Fig. 2a (a))/11-mercaptoundecanoic acid (11-MUA, Fig. 2a (b)). Then, biotin was covalently attached to the carboxylate groups using 1-ethyl-3-[3-dimethylaminopropyl] carbodiimide hydrochloride (EDC, Fig. 2a (c)). The number of resulting biotin sites will be determined by the yield of the EDC coupling reaction. A schematic illustration of the LSPR immunosensor depicting its exposure to streptavidin (SA) is shown in Fig. 2b.

Figure 2a shows surface chemistry of the Ag particle array-based immunosensor. A mixed monolayer of (a) 11-MUA and (b) 1-OT is formed on the exposed surfaces of the Ag nanoparticles followed by the covalent linking of (c)

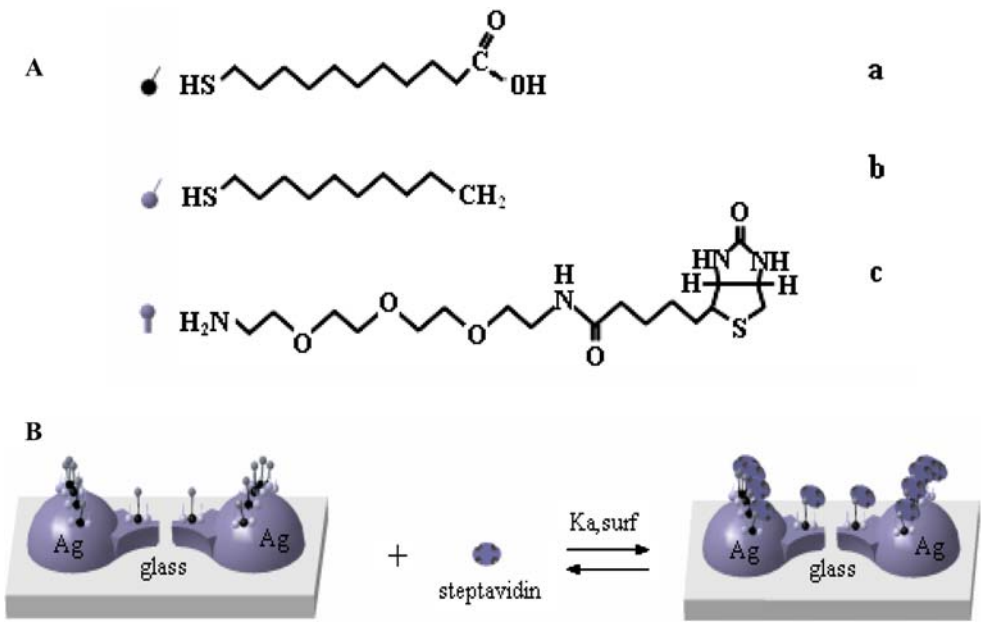

Fig. 2 **a** Surface chemistry of the Ag immunosensor, a mixed monolayer of (*a*) 11-MUA and (*b*) 1-OT is formed on the exposed surfaces of the Ag nanoparticles followed by the covalent linking of (*c*) biotin to the carboxyl groups of (*a*) 11-MUA; **b** schematic diagram of SA binding to a biotinylated Ag nanobiosensor fabricated by NSL on a glass substrate

biotin to the carboxyl groups of (a) 11-MUA. When we chose the biotin, we considered that, if we lengthen the arm of the biotin molecule, we can enlarge the binding space between the biotin and SA. The longer the arms of the antigen, the more significant the binding effect of the antigen-antibody will be. Hence, the lengthened arm of the biotin molecule can strengthen the binding effect of the antigen-antibody.

Figure 2b shows a schematic representation of SA binding to a biotinylated Ag immunosensor fabricated using NSL method on a glass substrate. Before the specific reaction between the biotin and streptavidin, surface chemistry of the Ag immunosensor is accomplished in advance.

Experimental setup

In order to clearly observe influence of the shape and period on probing characteristics of these biosensors, we measured their extinction spectra one-by-one array using a spectrometer. These spectra are measured by a Sciencetech spectrophotometer-based optical system.

Visible-IR transmittance spectra were taken using a white light source (400~700 nm) transmitted through a multimode optical fiber. The light exiting from the source fiber is focused onto the sample using collimating lens. Moving the sample stage can alter the focusing position of the incident light. The light is transmitted through the sample and is collected using an identical focus lens attached to the multimode fiber which is connected to a monochromator. The photomultiplier of the monochromator is connected to a personal computer and the transmittance spectrum can be directly shown on the screen of the computer. The measurement progress is divided into four steps: (1) confirm the scale of the incident wavelength, which ranges from 400 to 700 nm; (2) adjust the visible-IR transmittance; (3) scan the background optics without samples in the sample holder; and (4) put the sample to the corresponding holder and scan it. The sample is placed with top surface perpendicular to the incident light. Using Sciencetech spectrophotometer can make the test simple because the transmittance spectra are directly shown on the screen, and thus further data treatment is not necessary. The extinction spectra for each step are obtained by means of seeking the negative logarithm of transmittance.

Results and discussions

To observe the influence of the periods and the shapes on sensing characteristics of the biosensors, we measured their extinction spectroscopy of the target molecule (SA) with the same concentration. Peak wavelength and intensity of the extinction spectra are changed during each step of surface functionalization for the Ag nanoparticles. The incidence wavelength ranges from 400 to 700 nm. Before surface functionalization, the Ag nanoparticles were exposed to solvent as described above. The LSPR λ_{max} of the Ag nanoparticles was monitored during each surface functionalization step. Firstly, λ_{max} of the bare Ag nanoparticles was measured. To ensure a well-ordered SAM on the Ag nanoparticles, the sample was incubated in the thiol solution for 24 h. After careful rinsing and thoroughly drying using N_2 gas, the LSPR λ_{max} after modification with the mixed SAM was measured.

The LSPR λ_{max} peak shift corresponding to this surface functionalization step was calculated. After that, the biotin was covalently attached via amide bond formation with a two-unit poly(ethylene glycol) linker to carboxylated surface sites. The LSPR λ_{max} after biotin attachment was measured, corresponding to an additional shift. The LSPR nanosensor was prepared for exposure to the target analyte with the same concentration. Exposure to 100 nM SA resulted in an additional LSPR λ_{max} shift. The transmission and extinction spectra for different periods and shapes are shown in Figs. 3, 4, 5, and 6, respectively.

Shape tuning

To study the shape tuning performance, a total four shapes, hemisphere, cylindrical, triangular, and rhombic, were employed in our biosensing experiments. It can be seen from these extinction spectra that the maximal value (peak values) of each extinction spectrum has red-shifted corresponding to each step in the surface modification of the NSL-derived Ag nanoparticles so as to form a biotinylated Ag immunosensor and the specific binding of SA. Curves A in Figs. 3, 4, 5, and 6 show the extinction spectra of the bare Ag nanoparticles. Curves B in Figs. 3, 4, 5, and 6 show the extinction spectrum after the Ag nanoparticles which were modified with 1 mM 1:3 11-MUA/1-OT. Curves C in Figs. 3, 4, 5, and 6 show the extinction spectrum after the Ag nanoparticles which were modified with 1 mM biotin. Curves D in Figs. 3, 4, 5, and 6 show the extinction spectrum after the Ag nanoparticles which were modified with 100 nM SA. It can be seen from Figs. 3, 4, 5, and 6 that the shapes of the nanoparticles have obvious effect on peak value of the extinction spectra. The spectra are significantly tailored by the Ag nanoparticle arrays with different shapes. Generally speaking, for the SA-specific binding to the biotin, a red shift occurs during the binding processes for the fourth shapes and the detection sensitivity is 100 nM. This

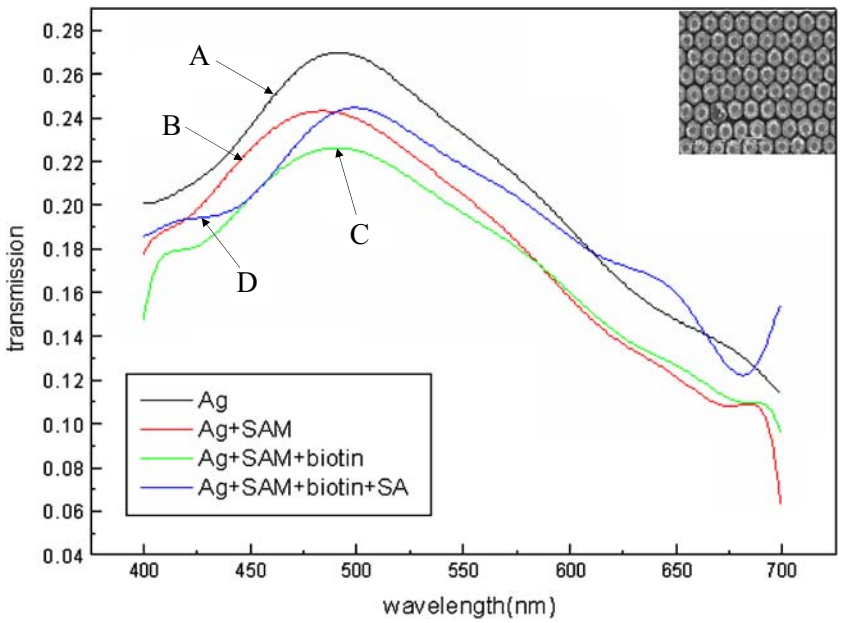

Fig. 3 Transmission spectra of each step for the surface modification using NSL-derived Ag hemisphere nanoparticle array with 440-nm period and form a biotinylated Ag immunosensor and the specific binding of SA. *Curve A*: Ag nanoparticles before chemical modification. *Curve B*: Ag nanoparticles after modification with 1 mM 1:3 11-MUA/1-OT. *Curve C*: Ag nanoparticles modified with 1 mM biotin. *Curve D*: Ag nanoparticles after modification with 100 nM SA. All transmission measurements were collected in air. Period of the array is 440 nm. The *inset* is an SEM micrograph of the fabricated Ag hemisphere nanoparticles

concentration is the same as the previous published results, but the multichannel-based optical biochip can realize detecting the various targeted molecular using the nanoparticle arrays with different shapes and periods simultaneously. When we used the Sciencetech spectrophotometer-based optical system to detect the visible-IR transmittance spectra of the LSPR-based biochip, the biochip is fixed in the holder, and the holder can be tuned in X and Y direction. Then, the transmission of different shape nanostructure arrays can be obtained directly.

Period tuning

Experimentally, the diverse diameters of the PS are used to adjust the period of the nanoparticle array. As experimental measurement examples, we gave extinction spectra from the hemisphere and triangular Ag nanoparticle arrays with period of 350 nm (previous period in Fig. 3 is 440 nm) and 500 nm (previous period in Fig. 5 is 440 nm) for the purpose of illustrating tuning role of the period of the nanoparticle arrays, as shown in Figs. 7 and 8. It can be

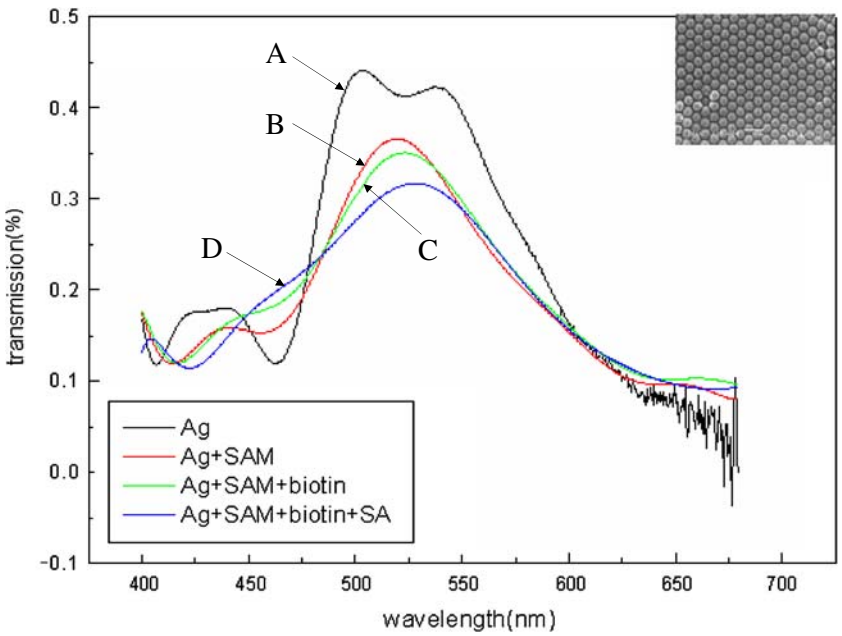

Fig. 4 Transmission spectra of each step for the surface modification using NSL-derived Ag cylindrical nanoparticle array with period of 500 nm and form a biotinylated Ag immunosensor and the specific binding of SA. *Curve A*: Ag nanoparticles before chemical modification. *Curve B*: Ag nanoparticles after modification with 1 mM 1:3 11-MUA/1-OT. *Curve C*: Ag nanoparticles modified with 1 mM biotin. *Curve D*: Ag nanoparticles after modification with 100 nM SA. All transmission measurements were collected in air. The *inset* is a SEM micrograph of the fabricated Ag column nanoparticles

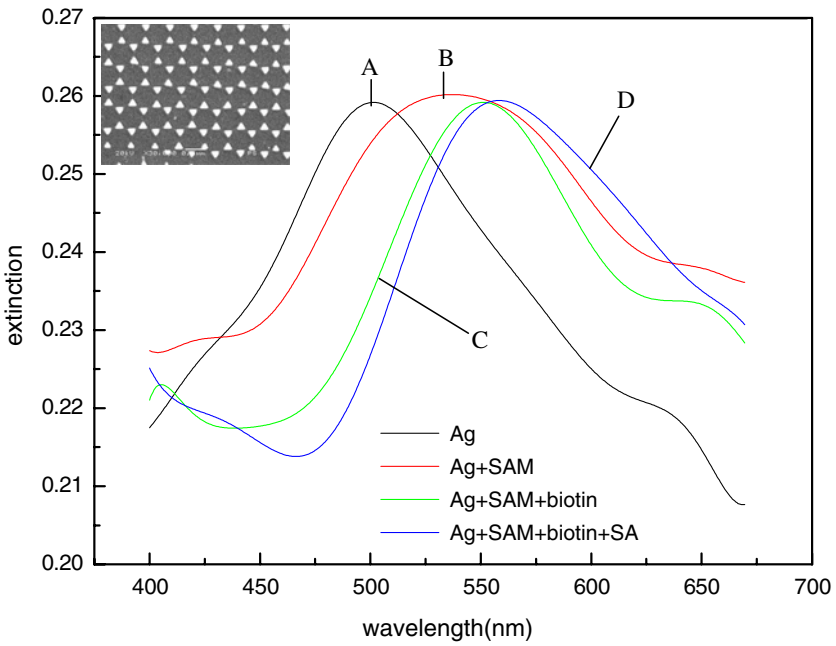

Fig. 5 LSPR spectra of each step for the surface modification using NSL-derived Ag triangular nanoparticle array with period of 440 nm, and form a biotinylated Ag immunosensor and the specific binding of SA. *Curve A*: Ag nanoparticles before chemical modification. *Curve B*: Ag nanoparticles after modification with 1 mM 1:3 11-MUA/1-OT. *Curve C*: Ag nanoparticles modified with 1 mM biotin. *Curve D*: Ag nanoparticles after modification with 100 nM SA. All transmission measurements were collected in air. The *inset* is an SEM micrograph of the fabricated Ag triangular nanoparticles

seen that the ~40-nm significant shifting of curves B, C, and D relative to curve A is observed. The period tuning effect is apparent compared to the peak shifting in Fig. 3. For the two arrays with 350-nm period hemisphere and 500-nm period triangular, a red shift still occurs while binding with SAM, biotin, and SA. However, for the 440-nm period hemisphere array, we observed one special case: a blue shift (see Fig. 3 case B). Further study is required to reveal this physical phenomenon.

In this experiment, it should be noted that all the extinction measurements were carried out in atmosphere environment. Therefore, the samples were contaminated by dust and water vapor of the ambient. In the future, the samples will be measured in airtight sample chamber which

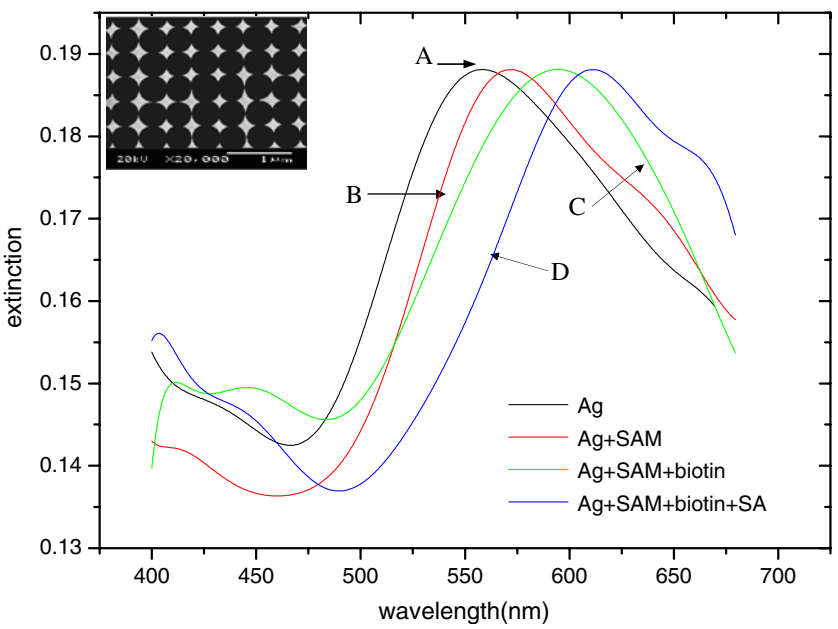

Fig. 6 LSPR spectra of each step for the surface modification using NSL-derived Ag rhombic nanoparticle array with 440-nm period and form a biotinylated Ag immunosensor and the specific binding of SA. *Curve A*: Ag nanoparticles before chemical modification. *Curve B*: Ag nanoparticles after modification with 1 mM 1:3 11-MUA/1-OT. *Curve C*: Ag nanoparticles modified with 1 mM biotin. *Curve D*: Ag nanoparticles after modification with 100 nM SA. All transmission measurements were collected in air. The *inset* is an SEM micrograph of the fabricated Ag rhombic nanoparticles

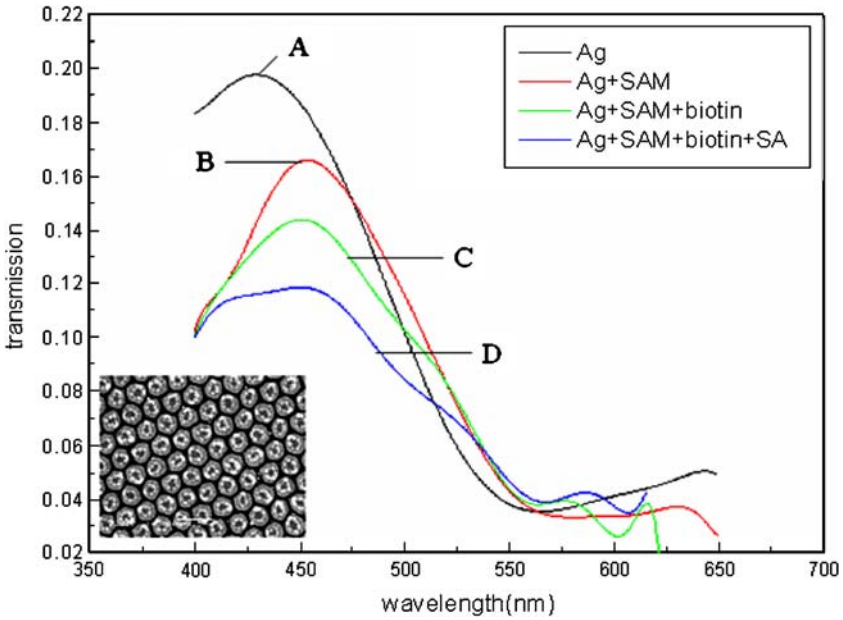

Fig. 7 Transmission spectra of each step for the surface modification NSL-derived Ag hemisphere nanoparticles, forming a biotinylated Ag immunosensor and the specific binding of SA. *Curve A*: Ag nanoparticles before chemical modification. *Curve B*: Ag nanoparticles after modification with 1 mM 1:3 11-MUA/1-OT. *Curve C*: Ag nanoparticles modified with 1 mM biotin. *Curve D*: Ag nanoparticles after modification with 100 nM SA. All transmission measurements were collected in air. Ag hemisphere array, period is 350 nm (previous period in Fig. 5 is 440 nm) and out-of-plane heights is 30 nm. The *inset* is an SEM micrograph of the fabricated Ag hemisphere nanoparticles with 350-nm period

is fully filled with N_2 gas. Theoretically, the detection sensitivity can be further improved.

Conclusions

A novel optical biochip with multichannels for detection of biotin–streptavidin on the basis of LSPR is put forth in this paper. To investigate sensing performance, we designed and fabricated the Ag nanostructure arrays with different shapes and periods as a biosensor with multichannels. Measurements of transmission and extinction spectra were carried out using the biosensors. Our spectroscopy results show that these LSPR-based nanoparticle arrays fabricated on a chip with different shapes and periods can be used as an immunosensor. Moreover, the optical biochip with multichannels can realize rapidly and mass detect the target molecule using the arrays with different shapes and periods simultaneously. This multichanneled biosensor has the advantages of time savings, high-throughput detection, and target selectivity in comparison to the traditional analysis methods.

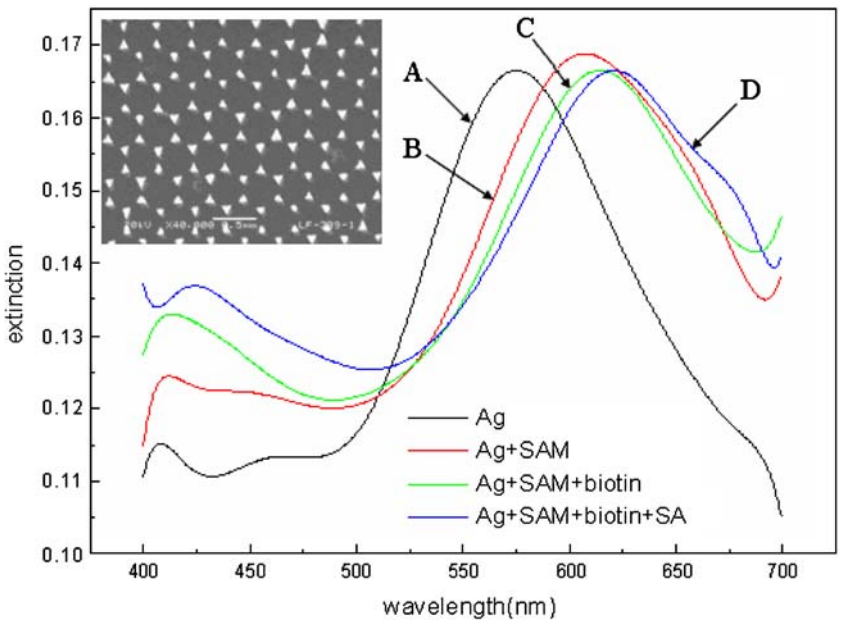

Fig. 8 LSPR spectra of each step for the surface modification NSL-derived Ag triangular nanoparticles, forming a biotinylated Ag immunosensor and the specific binding of SA. *Curve A*: Ag nanoparticles before chemical modification. *Curve B*: Ag nanoparticles after modification with 1 mM 1:3 11-MUA/1-OT. *Curve C*: Ag nanoparticles modified with 1 mM biotin. *Curve D*: Ag nanoparticles after modification with 100 nM SA. All transmission measurements were collected in air. Ag triangular array, period is 500 nm (previous period in Fig. 7 is 440 nm) and out-of-plane heights is 30 nm. The *inset* is an SEM micrograph of the fabricated Ag triangular nanoparticles with 500-nm period

Acknowledgment The work was supported by 973 program of China (no. 2006cb302900), "Distinguished Talent Program" from University of Electronic Science and Technology of China (no. 08JC00401), the National Natural Science Foundation of China (no. 60877021), and the innovation foundation of the Chinese Academy of Science.

Reference

1. Nakane J, Wiggin M, Marziali A (2004) Biophys J 87(1):615–621. doi:10.1529/biophysj.104.040212
2. Link S, El-Sayed M (1999) J Phys Chem B 103:8410–8426. doi:10.1021/jp9917648
3. Kelly KL, Coronado E, Zhao LL, Schatz GC (2003) J Phys Chem B 107:668–677. doi:10.1021/jp026731y
4. Link S, El-Sayed MA (2003) Annu Rev Phys Chem 54:331–366. doi:10.1146/annurev.physchem.54.011002.103759
5. Jackson JB, Halas NJ (2001) J Phys Chem B 105:2743–2746. doi:10.1021/jp003868k
6. Malinsky MD, Kelly KL, Schatz GC, Van Duyne RP (2001) J Am Chem Soc 123:1471–1482. doi:10.1021/ja003312a
7. Zhu SL, Li F, Luo XG, Du CL, Fu YQ (2008) Sens Actuators B Chem 134:193–198. doi:10.1016/j.snb.2008.04.028
8. Zhu SL, Li F, Luo XG, Du CL, Fu YQ (2008) Nanomedicine 3:669–677. doi:10.2217/17435889.3.5.669
9. Haes AJ, Van Duyne RP (2002) J Am Chem Soc 124:10596–10604. doi:10.1021/ja020393x
10. Haes AJ, Van Duyne RP (2003) Laser Focus World 39:153–156
11. Riboh JC, Haes AJ, McFarland AD, Yonzon CR, Van Duyne RP (2003) J Phys Chem B 107:1772–1780. doi:10.1021/jp022130v
12. Haes AJ, Zou S, Schatz GC, Van Duyne RP (2004) J Phys Chem B 108:109–116. doi:10.1021/jp0361327
13. Kawazumi H, Gobi KV, Ogino K, Maeda H, Miura N (2004) Chem Sens 20(Supplement B):794–795
14. Jung YJ, Oh MH, Lee SK, Taya M (2005) In: The 13th International Conference on Solid-State Sensors, Actuators and Microsystems, Seoul, Korea, June 5–9, pp 1800–1803
15. Zhu SL, Li F, Luo XG, Du CL, Fu YQ (2009) Opt Mater 31 (6):769–774. doi:10.1016/j.optmat.2008.07.014
16. Fu Y, Bryan NKA (2005) J Vac Sci Technol B 23:984–989. doi:10.1116/1.1926291
17. Fu Y, Bryan NKA, Zhou W (2006) J Nanosci Nanotechnol 6:1954–1960. doi:10.1166/jnn.2006.309